Dynamics of the population grating formation in erbium-doped fibers

E. Hernández Hernández, L. Martínez Martínez, and S. Stepanov
Centro de Investigación Científica y de Educación Superior de Ensenada, Ensenada, BC, 22860, México.

Received 28 July 2015; accepted 18 September 2015

Experimental results on formation dynamics of population gratings in erbium-doped fiber (EDF) investigated via two-wave mixing (TWM) are reported. It is shown that at all three utilized essentially different recording wavelengths 1492, 1526 and 1568nm the transient TWM response in EDF with low erbium concentration (≈ 640 ppm) has the characteristic rate significantly larger than that of the population of the Er^{3+} meta-stable level evaluated from the fluorescence dynamics. Additionally in EDF with high erbium concentration (≈ 5600 ppm) the TWM response is faster (even at low recording power) and the relative TWM amplitude is lower than that in EDF with low concentration. General increase of the TWM response rate is explained by contribution of a transient decrease of the fiber average absorption level, while above-mentioned differences observed in heavily doped EDF - by spatial migration of the excited states. The spectral dependence of the later effect is attributed to the difference in the absorption/emission cross-section ratio of the Er^{3+} ions at the utilized wavelengths.

Keywords: Dynamic population gratings; two-wave mixing; erbium doped fibers.

PACS: 42.65.Hw; 42.81.Wg; 78.47.jd

1. Introduction

Dynamic population gratings in the rare-earth-doped fibers [1], such as erbium- (EDF) and ytterbium- (YDF) doped, can be utilized in single-frequency fiber lasers [2-4], in adaptive interferometric sensors [5,6], for practical implementation of slow/fast light propagation [7,8] etc. For all these applications the amplitude of the reflection-type Bragg dynamic grating, recorded in the fiber by two counter-propagating mutually coherent waves, is of principal importance. It is well known, however, (see review paper [1] for details) that the recorded dynamic grating amplitude and, as a result, the efficiency of two-wave mixing (TWM) via these dynamic gratings are significantly lower than it can be estimated from spatially uniform saturation of the fiber optical absorption, gain, or refractive index. This discrepancy depends, however, on the recording wavelength and is minimal in the short-wavelength spectral region of the fundamental Er^{3+} ion optical absorption (1480-1490 nm) but can reach one order of magnitude in the central (around 1530nm) and in long-wavelength (1560-1570 nm) spectral regions [9].

Earlier attempts to attribute this discrepancy to the polarization mismatch between the recording waves [10], to the exited state absorption [11], or to the resonance frequency up-conversion [12,13] have failed to explain the experimentally observed reduction of the grating amplitude. Additionally, the exited state absorption and the resonance frequency up-conversion which lead to the fiber unsaturated absorption are to be also observed under spatially uniform illumination of the doped fiber.

The grating amplitude reduction can also be associated with the spatial migration of the excited state [14], which can be effective for the reflection Bragg grating with ≈ 0.5 μm (in the EDF case) fringe spacing, but is not important in case of the spatially uniform fiber excitation. Earlier this mechanism of the dynamic gratings reduction was reported to be effective in the bulk molecular and laser crystals with the saturable absorption [15,16]. The most important manifestation of the excitation migration effect in these experiments was fast increase of the grating relaxation rate with the reduced spatial spacing.

The doped fiber population gratings in question are usually recorded by two counter-propagating waves and the fringe spacing of the grating is practically impossible to change in a significant way since the recording wavelength inevitably is to be selected from the relatively narrow wavelength range (in particular, from 1480-1570 nm in EDF). For this reason, in Ref. 17 we have investigated dependence of the grating relaxation rate and amplitude in fibers with different erbium concentration. These first experiments have indeed demonstrated additional increase of the grating amplitude reduction and corresponding relaxation rate (by ≈ 30 %) in fibers with high (≈ 5600 ppm) erbium concentration but have failed to explain the general grating amplitude reduction in fibers with moderate erbium concentration (down to ≈ 640 ppm). The experiments were, however, performed at the wavelength 1550 nm only, and could not clarify dependence of the TWM efficiency on the recording wavelength.

Below in this paper we present the original experimental results on the grating formation rate and amplitude in fibers with two essentially different erbium concentrations but at three wavelengths 1492, 1526, and 1568 nm - from different parts of the Er^{3+} ions absorption spectrum. The obtained results are compared with the computer Monte Carlo simulation of the excited state migration in a random red of the ions with the average erbium concentrations corresponding to those in the real fibers utilized in our experiments.

2. Experimental samples and TWM results

The presented experimental results were obtained using commercial single-mode erbium-doped fibers Er103 and Er123

TABLE I. Experimentally measured optical characteristics of the EDF samples.

Fiber	$L(m)$	$\alpha_0 L$@ 1492 nm	P_{sat}@ 1492 nm (mW)	$\alpha_0 L$@ 1526 nm	P_{sat}@ 1526 nm (mW)	$\alpha_0 L$@ 1568 nm	P_{sat}@ 1568 nm (mW)
Er103	1.98	1.20	1.0	2.29	0.37	0.59	0.78
Er123	0.215	1.23	0.7	2.1	0.33	0.77	0.78

purchased from CorActive. To prevent erbium clustering, the fibers were also Al and Ge co-doped. These two fibers were selected because being otherwise approximately similar (with the core diameter of 4 ± 1 μm, confinement factor close to 1, and N.A. = 0.16) they have essentially different erbium concentrations which ensured their maximal optical absorptions of 4.5 and 43.3 dB/m (at 1532 nm). Using these absorption coefficients, other parameters of the fibers, and the maximum absorption cross-section $\sigma_a \approx 5.5 * 10^{-21}$ cm^2 of Er^{3+} ions [18] earlier in Ref. 17 we have evaluated the corresponding erbium concentrations as $\approx 1.6 * 10^{18}$ and $\approx 14 * 10^{18}$ cm^{-3} (≈ 640 and ≈ 5600 ppm), Note that taking into account the above-mentioned ambiguity in the fiber core diameter, provided by the producer, these evaluations of the erbium concentrations can be considered as having ± 50 % accuracy only.

To ensure similar conditions of the TWM experiments, we have prepared the samples of essentially different lengths L of 1.98 and 0.215 m for Er103 and Er123 fiber respectively. These were characterized by approximately similar initial (not saturated) optical density $\alpha_0 L$ - see Table I. The ends of the doped fiber segments were spliced with single-mode fiber SMF28 pieces terminated with APC connectors. Direct measurements with the optical spectrophotometer resulted in the maximum (at 1532 nm) fibers optical density $\alpha_{0\,\max} L$ about 2.6 and 2.5 respectively. It was found that the prepared fiber samples also have some background losses about 10% of the maximum value, which can be attributed to not ideal splicing and, partially, to the not-saturable absorption of the fiber.

In the presented experiments we utilized distributed-feedback (DFB) semiconductor lasers with $\approx$ 20 mW cw output at the wavelengths 1492, 1526, and 1568 nm. Direct measurements have demonstrated that the coherence length of these lasers is > 20 m that is clearly enough for the TWM experiments with the 1 m-long fibers. Initial optical densities of the utilized two fiber samples measured at these three operation wavelengths are presented in Table I.

Another very important characteristic of the fiber samples is their saturation power P_{sat}. This value is determined as the incident saturating light power P, which results in a two-fold reduction of the fiber optical absorption from its initial, not saturated value α_0:

$$\alpha = \frac{\alpha_0}{1 + P/P_{\text{sat}}} \tag{1}$$

Note that this and all the following theoretical equations was obtained for a two-level model, which seems to be adequate to the experimental situation under consideration, where no optical pumping is utilized and the erbium ion population is distributed between the fundamental and the meta-stable energy levels. In this approximation the dynamics of the saturated optical absorption and of the fluorescence is determined by the dynamics of population of the meta-stable level, *i.e.* is the same.

In a simple model of the non-interacting and collinearly oriented ions [19] the saturation power depends on the ion absorption and emission cross-sections (σ_a and σ_e respectively), the meta-stable state relaxation time τ_0, and the fiber effective modal area A:

$$P_{\text{sat}} = \frac{A\hbar\omega}{(\sigma_a + \sigma_e)\tau_0} \tag{2}$$

where $\hbar\omega$ is the incident light photon energy. More complicated analysis [20] shows, however, that additional numerical factor 2-4 is to be included in the right-hand side of this equation because of a random orientation of the active ions and the non-uniform distribution of the light power in the effective modal area.

Experimentally the saturation power can be evaluated from the incident power dependence of the optical absorption (see Eq. (1)), but also from a similar dependence of the fluorescence intensity and from the incident power dependence of its growth rate. If the fluorescence is measured in the transverse configuration (see Fig. 1a), these measurements give more correct data since they are taken from a small segment of the doped fiber where the excitation light power can be considered as a constant and equal to the incident one. The fluorescence intensity I_{fl} is obviously proportional to the population N_2 of the meta-stable level:

$$I_{fl} \propto N_0 \frac{P/P_{\text{sat}}}{2(1 + P/P_{\text{sat}})} \tag{3}$$

On the other hand, the growth rate for the meta-stable population (and, in this way, that of the fluorescence) is expressed by the following equation:

$$\tau^{-1} = \tau_0^{-1}(1 + P/P_{\text{sat}}) \tag{4}$$

In the below-presented experiments the fluorescence is excited by the incident light with the wavelength from the fundamental erbium absorption spectrum.

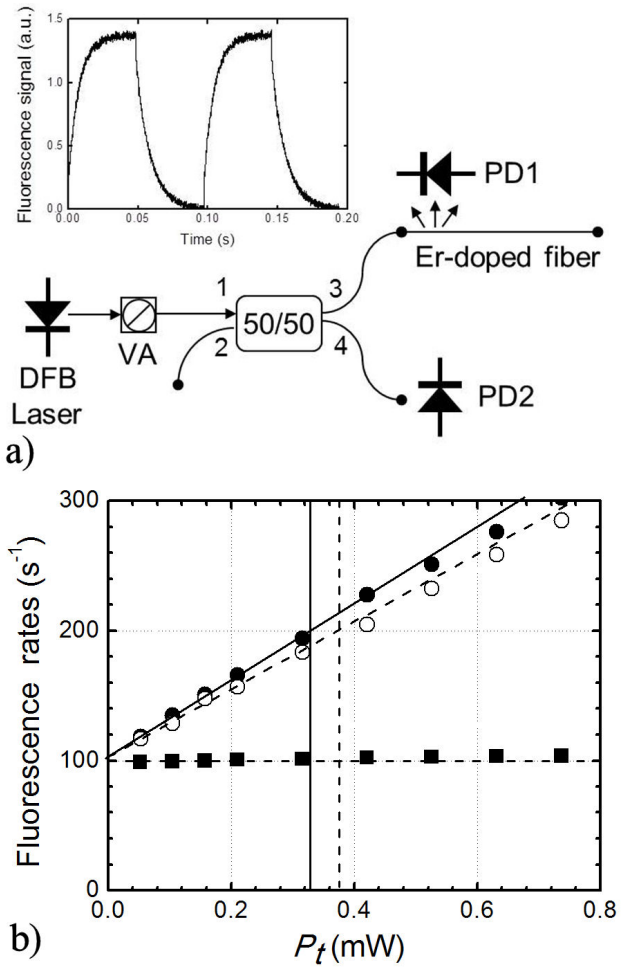

FIGURE 1. a) Experimental configuration utilized for transverse observation of the fluorescence signal in EDF. Inset shows the fluorescence signal shape in case of rectangular modulation of the incident light power (VA is the variable light attenuator, the photodiode PD1 is used for detection of the fluorescence signal, PD2 - for evaluation of the incident laser power). b) Incident power dependences of the fluorescence growth rate in Er103 and in Er123 fibers (empty and filled circles respectively) observed for excitation at 1526 nm. Filled squares show the fluorescence dark decay rate in Er123.

Figure 1b shows an example of the experimental dependences of the fluorescence growth rate (*i.e.* the inverse growth time) as a function of the incident light power for excitation with wavelength 1526 nm. For reference, the fluorescence dark decay rate (*i.e.* that observed without light), corresponding to the spontaneous relaxation rate of the Er^{3+} meta-stable level about 10 ms [18] is also presented (filled squares). The fitting values of the saturation powers, evaluated from the experimental curves using the theoretical dependence presented by Eq. (4), are also listed in Table I for all three excitation wavelengths. The obtained values of P_{sat} for different wavelengths correspond reasonably to the expected spectral dependence of $(\sigma_a + \sigma_e)^{-1}$ [18].

The TWM experiments [1] were performed in a conventional configuration (Fig. 2) with two counter-propagating

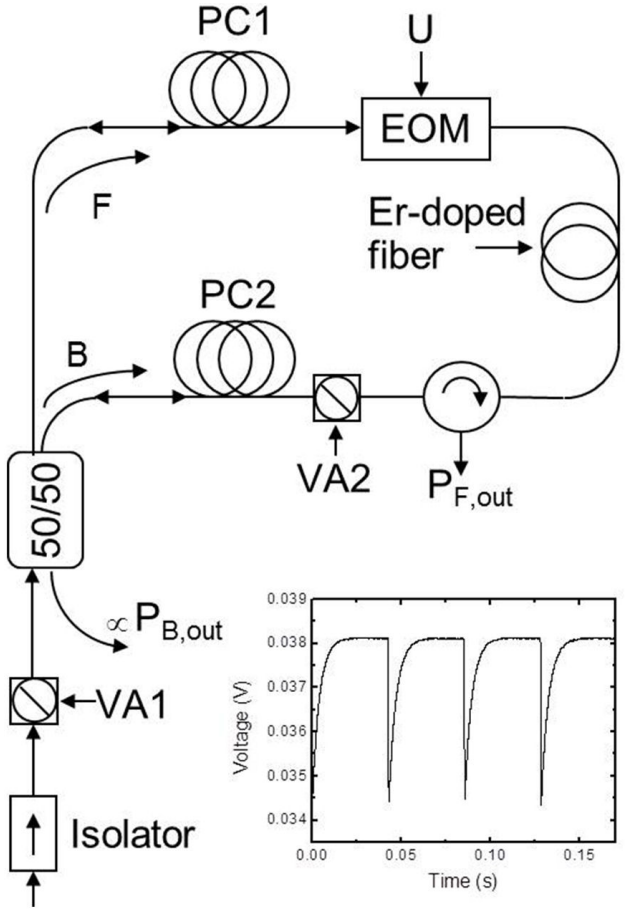

FIGURE 2. Experimental setup utilized for observation of the TWM signal via population dynamic grating in EDF (VA1,2 are variable attenuators, PC1,2 are polarization controllers, EOM is electrooptic modulator). Inset shows typical even response from the amplitude grating component effectively detected in case of $V_{\pi(p-p)}$ amplitude of the rectangular phase modulation.

through the doped fiber mutually coherent waves and with rectangular phase modulation introduced in one of them via electro-optic modulator. The incident power ratio between the two recording waves P_B/P_F was about 1 in this particular setup. The output TWM response, with the shape illustrated in the inset to Fig. 2, was detected in the output power of the recording wave F of the lower intensity. To eliminate TWM response from possible phase-type population grating [9] the peak-to-peak amplitude of the rectangular phase modulation was selected close to the half-wave voltage V_π. This ensured "even" shape of the detected TWM response with the equal amplitudes of two consequent negative TWM pulses typical for the amplitude dynamic grating. Polarization controllers (PC1 and PC2) were used to ensure proper light polarization at the input of EOM and equal similar light polarizations inside the doped fiber segment.

The experimentally observed TWM response was characterized by its maximal relative amplitude defined as a ratio $(\Delta V' = \Delta V/V_0)$ of the peak amplitude ΔV and the average transmitted signal V_0, and by the characteristic rate τ_g^{-1} (*i.e.* the inverse relaxation time). Experimental dependences of

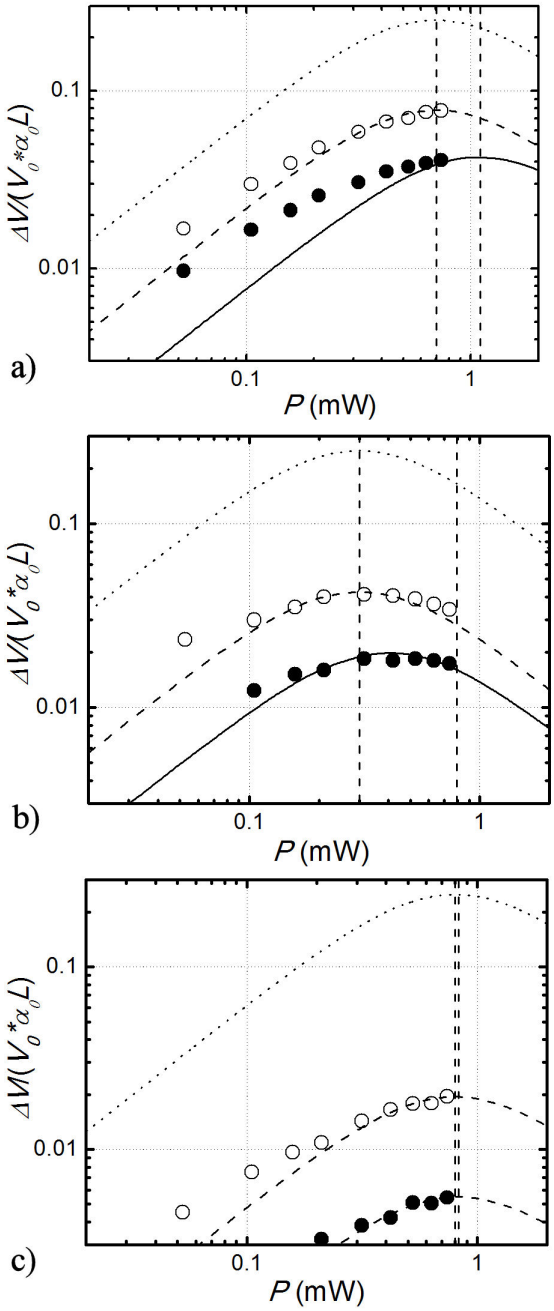

FIGURE 3. Incident power dependences of the TWM signal relative amplitude in Er103 and Er123 fibers (empty and filled circles respectively) obtained for different recording wavelengths (nm): 1492 - a) 1526 - b) and 1568 - c) (dotted line shows expected theoretical curve obtained in a approximation of low contrast grating).

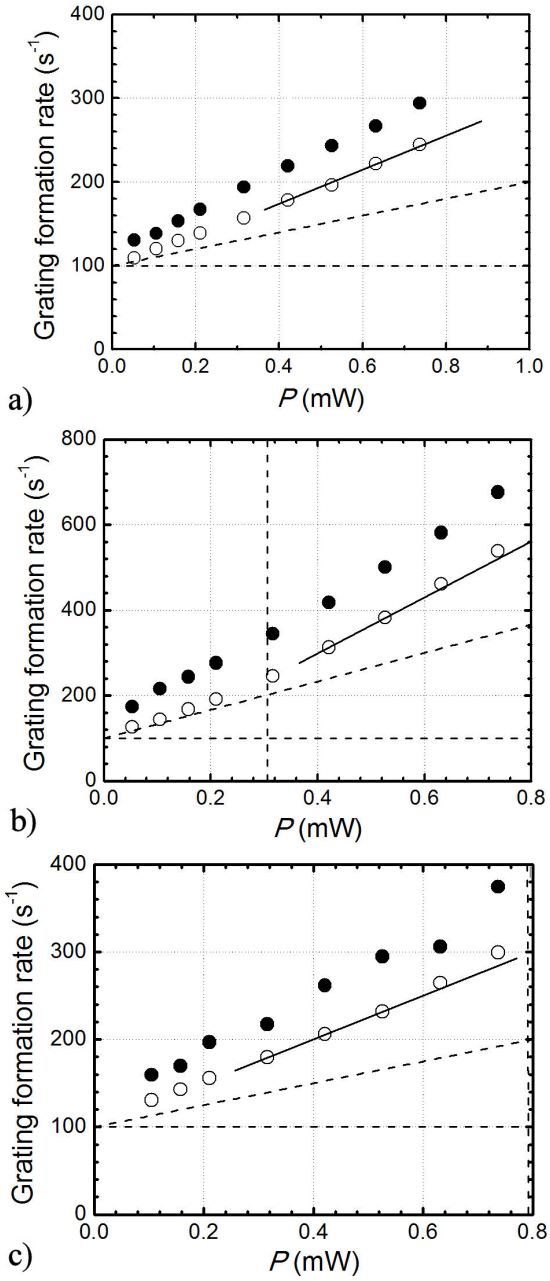

FIGURE 4. Incident power dependences of the TWM signal relaxation rate in Er103 and Er123 fibers (empty and filled circles respectively) obtained for different recording wavelengths (nm): 1492 - a), 1526 - b), and 1568 - c). Dash lines show the fluorescence growth/decay rates in Er103, and the solid lines has two times larger inclination as that of the fluorescence growth rate.

the TWM relative amplitude (normalized tambien to the initial fiber optical density) observed in fibers with different erbium concentration at all three operation wavelengths are presented in Fig. 3. At the horizontal axes of these dependences the total light power ($P = P_B + P_F$) incident to the doped fiber from both ends is presented. Figure 4 shows the corresponding experimental dependences of the TWM relaxation rate τ_g^{-1} on the total incident light power P.

3. Discussion

Dependences of the normalized amplitudes of the TWM signal on the average recording light power were analyzed in our earlier paper [21] (see also [1]). Note that in this theoretical consideration and the numerical simulations the attenuation of the incident recording waves, large-scale nonuniformity of

TABLE II. TWM relative amplitude reduction factors experimentally observed in fibers with different erbium concentration for different wavelengths.

Fiber	χ@ 1492 nm	γ@ 1492 nm	χ@ 1526 nm	γ@ 1526 nm	χ@ 1568 nm	γ@ 1568 nm
Er103	3.2	–	6.0	–	13	–
Er123	6.0	1.2	13	1.5	45	1.5

the doped fiber saturation, as well as the non-uniform profile of the recorded grating amplitude were taken into account. For the initial optical densities of the doped fiber $\alpha_0 L \leq 1$ and equal incident recording powers the maximal relative TWM signal amplitude observed for $V_{\pi p-p}$ phase modulation was approximated by the following dependence (dot lines in Fig. 3):

$$\Delta V' = \frac{\alpha_0 L}{2} \frac{P/P_{\text{sat}}}{1+(P/P_{\text{sat}})^2} \tag{5}$$

which is easily obtained from Eq. 1 in approximation of low contrast of the recording interference pattern. In case when one of the recording waves is significantly weaker than the other one and the output signal is detected in this weaker transmitted wave, an additional factor of 2 is to be added to the right hand side of Eq. 5 [22].

The theoretical dependence of the relative TWM signal amplitude (Eq. 5) shows an initial linear growth with the total incident power for $P < P_{\text{sat}}$, followed by the maximum value $(\alpha_0 L)/4$ observed at $P = P_{\text{sat}}$, and later by the inversely linear decay. Quantitatively, the predicted behavior is observed in the experimental dependences presented in Fig. 3. The maximum absolute values prove to be, however, well below the theoretical estimate $(\alpha_0 L)/4$. The numerical values of the reduction factor χ obtained in both investigated fibers for all the utilized wavelengths are given in Table II.

In Ref. 9 it was reported that the minimal reduction factor is observed at the shortest wavelength region of the Er^{3+} absorption spectrum, namely at 1492 nm in present experiments. As it was observed also in Ref. 17 for 1550 nm, the relative TWM signal amplitude is significantly larger in Er103 fiber with lower erbium concentration than in Er123. It is clear that the spectral dependence of the difference (*i.e.* the ratio) in χ factors between the fibers Er103 and Er123 (by factor 2.0 ± 0.1 at 1492 and 1526 nm and by factor 2.5 at 1568 nm) is, however, significantly weaker than the spectral dependence of the reduction factor χ itself.

As it is predicted by the theoretical analysis of the population grating formation in presence of the spatial migration of the excited states, the grating formation rate (and that of the TWM response) in fiber Er123 is faster than that in Er103 with lower erbium concentration - see Fig. 4. The factor γ of this growth of the grating relaxation rate in Er123 as compared with Er103 when approximated to low incident laser power is also presented in Table II.

This difference between the relaxation rate of the TWM signal in fibers with different erbium concentration will be discussed below in this Section. Let us begin our analysis with other obvious discrepancy between the relaxation rates of the TWM response and those of the fluorescence which in the above-presented Fig. 4 are marked by the dashed lines. It seems to be clear from this figure that the TWM rate is always larger than that of the fluorescence, while the relation between them is expected to be the opposite. Indeed, the fluorescence signal is detected from the initial segment of the fiber where the transmitted light power practically equals the total incident power. In its turn, the TWM signal is collected from the whole length of the fiber, when, on average, because of the fiber absorption, the local value of the transmitted power can be significantly lower than the total power incident from both fiber ends. Only if the incident power is significantly larger that the saturation power of the fiber, when the fiber absorption is saturated, the TWM relaxation rate with the incident light power is expected to reach that of the fluorescence growth.

The above-mentioned expected behavior was reported in our earlier publication [17], where significantly different recording light powers entering the fiber from the opposite ends were utilized. In the presented experiments, the behavior of the TWM rate is significantly different: it seems that for the TWM the effective saturation power of the fiber is approximately two times smaller. We can explain this discrepancy by the fact that the present TWM mixing experiment is performed with approximately equal recording light powers. In this case the average contrast of the recorded grating is very close to 1, and it is necessary to take into account nonlinear effects accompanying the grating formation.

Indeed, in the interference pattern of a large contrast m, the relaxation of the fiber optical absorption, leading to formation of the amplitude population grating, is an essentially nonuniform process, and the grating profile is far from the sinusoidal one. In particular, Fig. 5a shows temporal evolution of one grating spatial period profile after the π step-like displacement of the interference pattern of a large contrast ($m = 0.9$) utilized in our TWM experiments. The fundamental Bragg spatial component of the grating responsible for the TWM interaction relaxes with the expected rate of the fluorescence growth rate (see Eq. 4). What is important, that along with the re-recording of the grating for a new position of the interference pattern, the average level of the fiber optical absorption experiences some transient temporal drop - see Fig. 5b. Unlike the amplitude of the Bragg grating component which is approximately proportional to the interference

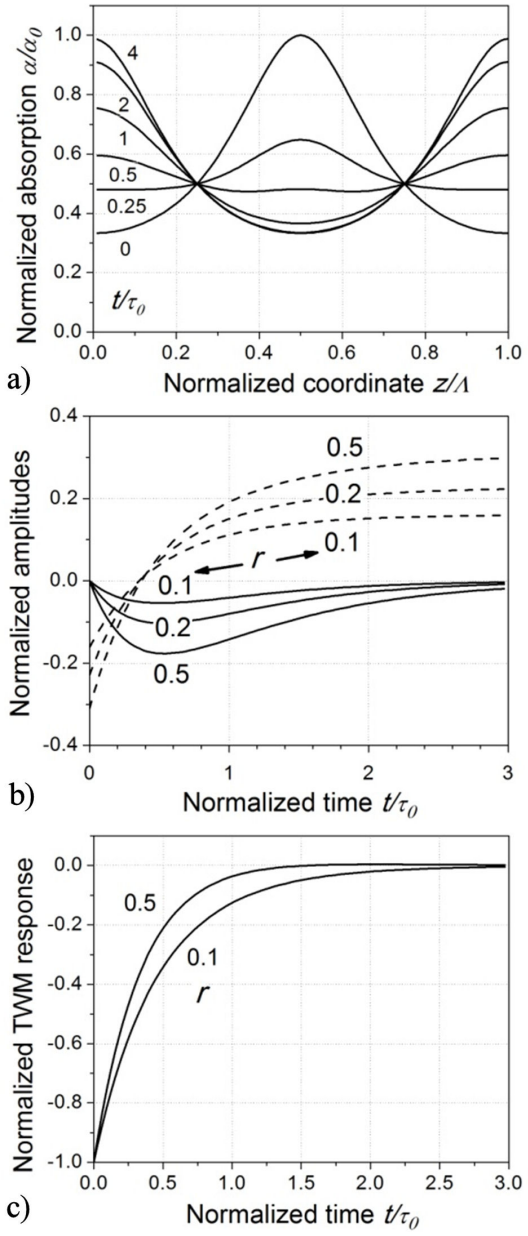

FIGURE 5. Temporal evolution of the fiber absorption coefficient after the step-like π-shift of the recording interference pattern a). Temporal variation of the Bragg component in the absorption grating (dashed lines) and of the variable part of the average absorption (solid line, multiplied by 3) for different incident recording powers ratio $r = P_F/P$ b). Normalized TWM response profiles observed for 0.5 and for 0.1 r values c). All figures were obtained for $P/P_{\text{sat}} = 1$.

pattern contrast m, the amplitude of the average level drop is quadratic on it (see also Fig. 5b), *i.e.* is insignificant at low contrasts of the recording pattern. Note that similar transient component is also observed in the fluorescence intensity, when it is observed in the process of the TWM experiment [23].

Along with the transient self-diffraction from the grating Bragg component, this drop in the average absorption contributes to formation of the TWM signal, due to direct modulation of the transmitted waves. The analysis shows that, as a result of this, in case of equal recording wave powers the experimentally observed response demonstrates approximately 1.5-2-time larger relaxation rate - Fig. 5c. On the opposite, when the incident recording light powers are significantly different, the interference pattern contrast goes down and the TMW response observed in the transmitted low power wave has the relaxation rate equal to that of the fluorescence (Eq. 4).

Clearly, in a more detailed analysis of this effect one has also take into account the spatial nonuniformity in average recording power, saturated optical absorption, and the interference pattern contrast along the fiber length. Here we use this argument to explain quantitatively the experimentally observed increased relaxation rates of the TWM responses. Indeed, as one can see from Fig. 4, the experimental points observed for TWM in Er103 fiber at large incident powers are much better approximated with the linear dependences (solid lines) growing two times faster than those of the fluorescence (dashed lines in the same figures). As it was mentioned above, slowing down of this growth at low incident light intensities is explained by initial optical absorption of the doped fibers, which leads to an effective reduction of the total light power along the fiber length.

In accordance with the theoretical analysis of the population grating formation in presence of the excited state migration [15,16], the grating relaxation rate at low recoding power ($P \ll P_{\text{sat}}$) is to be increased by the factor:

$$\varsigma = (1 + K^2 L_D^2) \tag{6}$$

where $K = 2\pi/\Lambda$ is the wave-number of the recorded Bragg grating (about $(4\pi n/\lambda) \approx 12\ \mu\text{m}^{-1}$ in our case). It is to be also accompanied by a similar reduction of the steady-state grating amplitude and by corresponding reduction in the transient TWM response.

Simple analysis presented in Ref. 24 of the random distributions of the erbium ions with average erbium concentration of Er103 fiber shows that only a small fraction of the erbium ions (about 13%) have another ions closer than the Forster radius $R_0 \approx 2$ nm for the erbium ions in EDF [13,25]. This means that we can practically neglect the influence of migration of the excited states on the grating formation in this EDF. This conclusion is, in particular, confirmed by the fact (see Fig. 4) that, when approximated to the lower incident power, the TWM response relaxation rate in Er103 is about $\tau_0^{-1} \approx 100\ \text{s}^{-1}$.

On the opposite, for the erbium concentration in Er123 fiber, the similar analysis shows that the majority of the ions have closest neighbors with the distances less than R_0 that means that the excited state migration can influence in the grating formation in this fiber significantly. And indeed, experimentally we observe additional increase in the grating formation rate in this fiber as compared with Er103, even at very low recording power - see Fig. 4.

Comparing the theoretical factor expressed by Eq. 6 with the experimentally observed values of γ from the Table II we obtain that the diffusion length L_D in Er123 is changing in the range 40-60 nm in the investigated wavelength region 1492-1568 nm. This evaluation corresponds quite well to our earlier estimate of $L_D \approx 48$ nm obtained for similar fiber Er123 at 1550 nm in Ref. 17.

As it was mentioned above, the growth in the grating formation rate due to spatial migration of the excited state is to be associated with the proportional reduction of the steady-state population grating amplitude. And indeed, in the above-presented experimental results (see Table II) the TWM signal in Er123 is significantly lower than that in Er103. The experimentally observed grating amplitude reduction (by factor 1.9 – 2.5) is, however, larger than similar increase in the grating formation rate (factor 1.2 – 1.5). The spectral dependences of these variations correspond, however, to each other quite well: at the wavelength 1492 nm both factors are minimal, and at 1568 nm both are maximal.

As we have evaluated in Ref. 17, the absolute value of the erbium concentration in fiber Er123 is about $5.6*10^{19}$ cm^{-3}. For a generally accepted in current literature Forster radius $R_0 \approx 2$ nm this corresponds to the normalized (to R_0^3) average erbium ion concentration $C \approx 0.5$. For this value of C our numerical simulations based on the Monte Carlo algorithm resulted in the excitation diffusion length equal to ≈5 nm. The above-presented erbium concentration was evaluated in Ref. 17 without taking into account the non-uniform distribution of light power in the fiber mode cross-section and of random orientations of the erbium ions in the silica core. If we take into account these factors [20], this can increase the evaluation of concentration by $\approx 3-4$ times and increase the diffusion length to ≈ 10 nm.

This estimate of L_D seems to be still rather far from the expected from our experimental measurements range of 40-60 nm. We can mention here that a simple increase of the Forster radius to 3 nm results in a feather significant growth ($\propto R_0^{5/2}$ of the expected diffusion length L_D to the value of ≈ 30 nm. Another physical reason which can lead to increasing of the effective diffusion length is associated with possible grouping of the erbium ions in a long chains or large clusters - the effect for which co-doping of EDFs with Al and Ge is utilized. Taking also into account the above-mentioned possible deviations in the fiber core area (by nearly 50% in accordance with the data supplied by the provider) or in the erbium confinement factor, we can state that our theoretical evaluation of the excitation diffusion length is in a reasonable agreement with the experimental data on the TWM response acceleration in our heavily doped fiber Er123.

Note that relatively small values of the excitation diffusion lengths evaluated both theoretically and experimentally even for heavily doped EDFs follow from the relatively low concentration of erbium which can be accepted by the amorphous silica matrix without forming of the erbium pairs or small clusters. For comparison, in the crystal matrices, where concentration of the rare-earth dopant can be much higher, the experiments with dynamic population gratings give significantly larger evaluations for excitation diffusion lengths. In particular, the excited state diffusion length among the Tm^{3+} ions of about 0.1 μm was reported in Ref. 16 for Tm,Ho co-doped YAG with thulium concentration approaching 10^{21} cm^{-3}.

The spectral dependences of factors χ and ζ can be explained within the framework of spatial migration of excitation in the following way. At short-wavelength end of the investigated spectral region the absorption crossection of Er^{3+} ions is significantly larger than the emission crossection ($\sigma_a > \sigma_e$), and at long-wavelength spectral end the situation is the opposite ($\sigma_a > \sigma_e$) [18]. The population gratings usually reach their maximum at the light power close to the saturation power at the recording wavelength (see Fig. 3). As a result, in the former case (at 1492 nm) relatively large fraction of the ions are excited (indeed, the EDF can even be inverted at this wavelength), but in the latter case (at 1568 nm) the majority of the ions are in base state. One can assume that in the second case the excited states have much more not excited neighbor ions to migrate, that obviously facilitates migration process for longer distances and wash out the spatial pattern of the grating more effectively.

4. Conclusions

Summarizing, we have presented the original experimental results of investigation of the dynamics of formation and of the amplitude of the population gratings in erbium-doped fiber (EDF) at three essentially different wavelengths 1492, 1526 and 1568 nm. It is shown that at all three wavelengths the dynamic grating in EDF are formed with the characteristic rate faster than that of population of Er^{3+} meta-stable level. Additionally, the grating formation rate in EDF with higher erbium concentration is always higher than in the fiber with low erbium concentration. In the same time, the steady-state grating amplitude in the fiber with larger erbium concentration was lower than that in EDF with lower concentration. General increase of the TWM response rate was explained by contribution of a transient decrease of the fiber average absorption level observed basically at high contrast of the interference pattern. Additional changes in TWM in heavily doped EDF are explained by spatial migration of excitation, which is inefficient in EDF with low erbium concentration. The spectral dependences of the observed effects associated with migration are explained by difference in the ratio of the absorption and emission cross-sections of Er^{3+} ions. Experimental evaluation of the excitation diffusion length (40-60nm) in the heavily doped fiber proved to be in a reasonable agreement with results of numerical Monte Carlo simulations.

1. S. Stepanov, *J. of Physics D* **41** (2008) 224-002.
2. M. Horowitz, R. Daisy, B. Fischer and J. Zyskind, *Electron. Lett.* **30** (1994) 648-649.
3. R. Paschotta, J. Nilsson, L. Reekie, A.C. Tropper, and D. C. Hanna, *Opt. Lett.* **22** (1997) 41-43.
4. Sh. Huang, G. Qin, A. Shirakawa, M. Musha, and K.-I. Ueda, *Opt. Express* **13** (2005) 7113-7117.
5. S. Stepanov, F. Pérez Cota, A. Nuñez Quintero, and P. Rodríguez Montero, *J. of Holography and Speckle* **5** (2009) 303-309.
6. J. López Rivera, M. Plata Sánchez, A. Miridonov, and S. Stepanov, *Opt. Express* **21** (2013) 4280-4290.
7. S. Stepanov and E. Hernández Hernández, *Opt. Lett.* **33** (2008) 2242-2244.
8. S. Stepanov and M. Plata Sánchez, *Phys. Rev. A* **80** (2009) 053830.
9. S. Stepanov and E. Hernández Hernández, *Opt. Commun* **271** (2007) 91-95.
10. S. Stepanov, E. Hernández, and M. Plata, *JOSA B* **22** (2005) 1161-1167.
11. A.D. Guzman-Chávez, Yu. O. Barmenkov, and A.V. Kir'yanov, *Appl. Phys. Lett.* **92** (2008) 191-111.
12. E. Delevaque, T. Georges, M. Monerie, P. Lamouler, and J. F. Bayon, *IEEE Photon. Technol. Lett.* **5** (1993) 73-75.
13. J. L. Philipsen and A. Bjarklev, *IEEE J.of Quant. Electron.* **33** (1997) 845-854.
14. R.C. Powell, *Physics of solid-state laser materials* (Springer, NY, 1998).
15. J.R. Salcedo, A.E. Siegman, D.D. Dlott, and M.D. Fayer, *Phys. Rev. Lett.* **41** (1978) 131-134.
16. V.A. French and R.C. Powell, *Opt. Lett.* **16** (1991) 666-668.
17. S. Stepanov and E. Hernández, *Opt. Lett.* **30** (2005) 1926-1928.
18. E. Desurvire *Erbium-doped Fiber Amplifiers. Principles and Applications* (Wiley InterScience, Inc., Hoboken, 2002).
19. A.E. Siegman, *Lasers* (University Science Books, Sausalito, 1986).
20. S. Stepanov, L. Martínez Martínez, E. Hernández Hernández, P. Agruzov, and A. Shamray, *J. Optics* **17** (2015) 075401.
21. S. Stepanov and C. Nuñez Santiago, *Opt. Commun.* **264** (2006) 105-115.
22. S. Stepanov and F. Pérez Cota, *Opt. Lett.* **32** (2007) 2532-2534.
23. S. Stepanov and E. Hernández *JOSA B* **24** (2007) 1262-1267.
24. L.O. Martínez-Martínez, E. Hernández-Hernández, and S. Stepanov, *Rev. Mex. Fis.* **59** (2013) 302-308.
25. D. Khoptyar, J. Gierschner, and H.-J. Egelhaaf *JOSA B* **24** (2007) 1527-1534.